Volume 46
Number 10
14 March 2017
Pages 3073-3412

Dalton Transactions

An international journal of inorganic chemistry

rsc.li/dalton

COMMUNICATION
Douglas W. Stephan et al
N-Heterocyclic carbene stabilized parent sulfenyl, selenenyl, and tellurenyl cations (XH+, X = S, Se, Te)

ISSN 0306-0012

ROYAL SOCIETY OF CHEMISTRY

This is an Accepted Manuscript, which has been through the Royal Society of Chemistry peer review process and has been accepted for publication.

Accepted Manuscripts are published online shortly after acceptance, before technical editing, formatting and proof reading. Using this free service, authors can make their results available to the community, in citable form, before we publish the edited article. We will replace this Accepted Manuscript with the edited and formatted Advance Article as soon as it is available.

You can find more information about Accepted Manuscripts in the Information for Authors.

Please note that technical editing may introduce minor changes to the text and/or graphics, which may alter content. The journal's standard Terms & Conditions and the Ethical guidelines still apply. In no event shall the Royal Society of Chemistry be held responsible for any errors or omissions in this Accepted Manuscript or any consequences arising from the use of any information it contains.

ROYAL SOCIETY OF CHEMISTRY

rsc.li/dalton

Computational demonstration of Isomer- and spin-state-dependent charge transport in molecular junctions composed of charge-neutral iron(II) spin-crossover complexes

Nicolás Montenegro-Pohlhammer,[a,b]* Senthil Kumar Kuppusamy,[c]* Gloria Cárdenas-Jirón,[a] Carmen J. Calzado[b] and Mario Ruben[c,d,e]

[a]Laboratory of Theoretical Chemistry, Faculty of Chemistry and Biology, University of Santiago de Chile (USACH), 9170022, Santiago, Chile.

[b]Departamento de Química Física. Universidad de Sevilla. c/ Profesor García González, s/n. 41012 Sevilla. Spain.

[c]Institute of Quantum Materials and Technologies (IQMT), Karlsruhe Institute of Technology (KIT), Karlsruhe, Germany.

[d]Institute of Nanotechnology, Karlsruhe Institute of Technology (KIT), Karlsruhe, Germany.

[e]Centre Européen de Sciences Quantiques (CESQ), Institut de Science et d'Ingénierie Supramoléculaire (ISIS), Université de Strasbourg, Strasbourg, France.

*Authors to whom the correspondence should be addressed

Email: nicolas.montenegro.p@usach.cl, senthil.kuppusamy2@kit.edu.

Abstract

Chemistry offers a multitude of opportunities towards harnessing functional molecular materials with application propensity. One emerging area of interest is molecular spintronics, in which charge and spin degrees of freedom are used to achieve power-efficient device architectures. Herein, we show that, with the aid of state-of-the-art quantum chemical calculations on designer molecular junctions, the conductance and spin filtering capabilities are determined by the molecular structure. As inferred from the calculations, structural control over the transport can be achieved by changing the position of the thiomethyl (SMe) anchoring groups for Au(111) electrodes in a set of isomeric 2,2`-bipyridine-based metal coordinating ligand entities L1 and L2. The computational studies on heteroleptic iron(II) coordination complexes (1 and 2) composed of L1 and L2 reveal that switching the spin-state of the iron(II) centers, from the low-spin (LS) to high-spin (HS) state, by means of an external electric field stimulus, could, in theory, be performed. Such switching, known as spin-crossover (SCO), renders charge transport through single-molecule junctions of 1 and 2 spin-state-dependent, and the HS junctions are more conductive than the LS junctions for both complexes. Additionally, the LS and HS junctions based on complex 1 are more conductive than those featuring complex 2. Moreover, it is predicted that the spin filtering efficiency (SFE) of the HS junctions strongly depends on the bridging complex geometry, with 1 showing a voltage-

dependent SFE, whereas 2 exhibits an SFE of practically 100% over all the studied voltage range. To be pragmatic towards applications, the ligands L1 and L2 and complex 1 have been successfully synthesized, and the spin-state switching propensity of 1 in the bulk state has been elucidated. The results shown in this study might lead to the synthesis and characterization of isomeric SCO complexes with tuneable spin-state switching and charge transport properties.

Introduction

Using molecules as circuit elements for fabricating realistic devices capable of performing the functions of traditional silicon-based transistors is the goal of molecular electronics and spintronics. Such a goal can only be achieved by studying how molecules respond to external triggers at the single-molecule level. In molecular electronics, the charge degree of freedom is leveraged to perform device operations, and charge transport across a molecular junction is controlled by varying the electrode-molecule coupling, which in turn can be achieved by tuning the molecular structure, as elucidated by Venkataraman and co-workers, for example.[1]

In molecular spintronics, the spin magnetic moment of carriers is used as a second degree of freedom along with the charge degree of freedom. Therefore, to fabricate molecular spintronics elements, control over both charge and spin degrees of freedom is necessary. Lanthanide- and transition-metal-based molecular complexes carrying magnetic spin degrees of freedom are ideally suited to serve as spintronics elements. Single-molecule magnets (SMMs) and spin-crossover (SCO) complexes are two different classes of spin-bearing molecular systems, whose utility has been demonstrated as spintronics elements.[2-4] In the case of SMMs, the anisotropic nature of the magnetic spin degree of freedom has been exploited to perform spin selective operations—a remarkable example is the [TbPc$_2$]-SMM-based molecular spin valve.[5] On the other hand, the spintronics utility of the SCO complexes stems from the spin-filtering characteristic of high-spin complexes in molecular junctions. The SCO complexes undergo high-spin (HS)-to-low-spin (LS), and vice versa, spin-state switching in the bulk[6-8] and thin-film[9-11] states, and at the single-molecule level.[12-14] The spin-state switching in the thin-film[15] and single-molecule[16] levels are shown to involve concomitant conductance switching and spin-filtering efficiency (SFE); thereby, a reversible ON-OFF switching of conductance and SFE can be achieved, assisting the progress toward the realization of switchable molecular spintronics architectures.

Charge neutral iron(II) complexes composed of sulphur-based anchoring groups are suitable for studying charge and spin transport characteristics at the single-molecule level. Complexes belonging to

[Fe(H$_2$Bpz$_2$)$_2$(L)]—H$_2$Bpz = dihydrobis(pyrazolyl)borate, L = 1,10-phenanthroline (phen) or 2,2'-bipyridine (bipy)—family[17,18] are useful candidates for developing molecular spintronics elements because the complexes can be functionalized with molecular anchoring groups for electrodes[19, 20], facilitating studies at single-molecule junctions. Although computational and experimental studies demonstrating spin-state-dependent conductance switching and spin-filtering nature of single SCO molecule junctions have been reported,[21-23] single-molecule level studies focusing on the [Fe(H$_2$Bpz$_2$)$_2$(L)] family of complexes are limited to a handful of studies in scanning tunneling microscopy (STM) junctions.[24-26] A notable example is the electron-induced SCO phenomenon demonstrated for [Fe(H$_2$Bpz$_2$)$_2$(phen)] in an STM junction.[27] Moreover, most of the studies relied on prototypical [Fe(H$_2$Bpz$_2$)$_2$(L)] complexes first reported by Real and co-workers[17], and structural diversity of [Fe(H$_2$Bpz$_2$)$_2$(L)]-based complexes is rather limited, when molecular spintronics application is concerned. Crucially, reports detailing single-molecule transport characteristics of anchoring group tethered functional [Fe(H$_2$Bpz$_2$)$_2$(L)] complexes are yet to be reported, to the best of our knowledge.

To elucidate the utility of the [Fe(H$_2$Bpz$_2$)$_2$(bipy)]-based complexes as molecular spintronics elements, we have computationally studied, using the nonequilibrium Green functions formalism combined with the density functional theory (NEGF-DFT), the transport characteristics of thiomethyl (SMe) anchoring group tethered charge neutral iron(II) complexes 1 and 2 based on ligands L1 and L2, respectively (Figure 1). Complexes 1 and 2 feature the 4-(methylhio)phenylethynyl anchoring groups at the 5,5′ and 4,4′ positions, respectively, of the 2,2'-bipyridine skeleton. The ligands and complexes featuring the same molecular formula are positional isomers, considering the different arrangements of anchoring groups on the 2,2'-bipyridine skeleton.

Our studies reveal that in the junctions composed of complex 1 or 2, the HS state is more conductive than the LS state. The HS-junctions show SFEs in the low bias regime reaching values of about 80% and 100% for 1 and 2, respectively, at 0.3 V. The spin-state-dependence of conductance and differing SFEs predicted for 1 and 2 indicate that the spin transport characteristics are completely determined by the molecular structure and spin-state. Crucially, we show that applied voltage has an effect on the frontier molecular orbitals of the complexes, dramatically changing the transport properties of the junctions, suggesting that it is possible to induce spin-state switching in the junctions of 1 and 2 by applying an electric field, implying the possible utility of the complexes as spintronics elements. Finally, by comparing the transport characteristics of LS-junctions of 1 and 2 with the respective constituent ligands L1 and L2, insights into

the role of the iron(II) centre in mediating charge transport have been obtained. Moreover, to show how the molecular functionalization affects the electronic structure and the resultant spin-state switching characteristics, the results obtained for 1 and 2 are compared with the prototypical [Fe(II)(H$_2$Bpz$_2$)$_2$(bipy)] complex, hereafter referred as complex 3 (Figure 1).

To be more practical in terms of device applications, we have attempted to synthesize the ligands and complexes discussed in this study. Our attempts were successful in the cases of L1, L2, and complex 1; whereas, a satisfactory characterization of complex 2 was not achieved. Nevertheless, our DFT-based thermo-chemistry calculations show that complex 2 has a negative ΔG of formation (G = standard Gibbs free energy), indicating that the compound is thermodynamically stable.
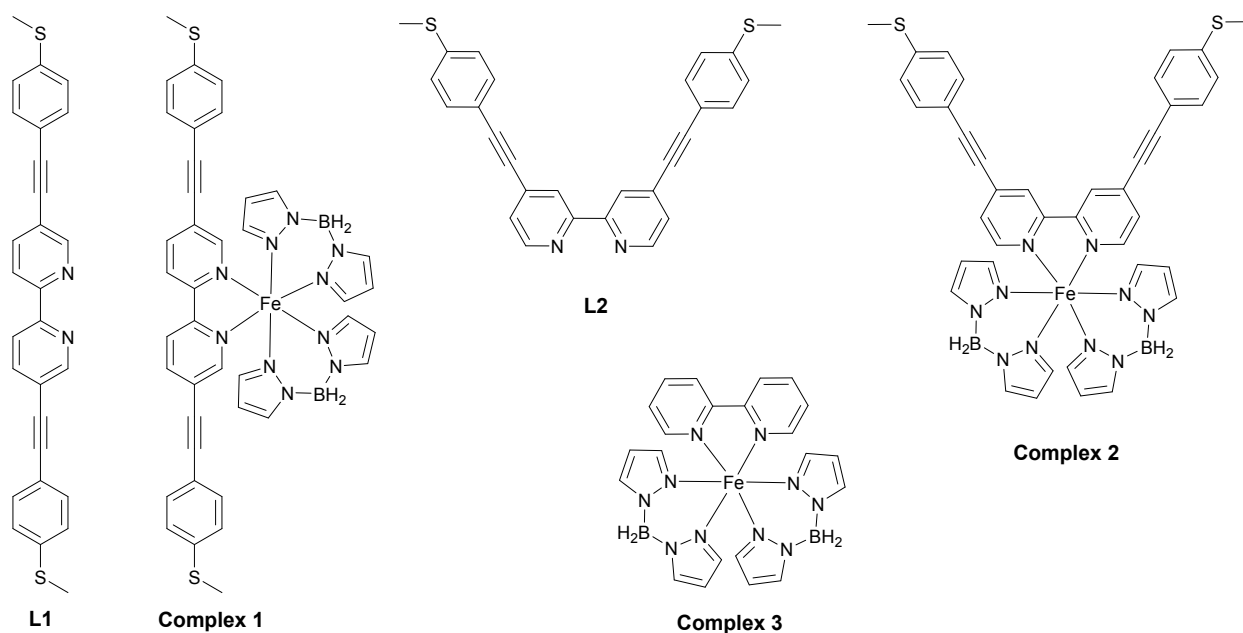

Figure 1. Molecular structures of the ligands (L1 and L2) and complexes (1, 2, and 3) discussed in this study.

Experimental procedures

Materials, experimental protocols, and instrumentation used to characterize the molecular systems are described in section S1 of the supporting information (SI).

Computational details

Electronic structure and magnetic properties of the complexes

The electronic structure and magnetic properties of complexes 1, 2, and 3 were calculated through Density Functional Theory (DFT) and Wave Function (WFT)-based methods, by means of the ORCA[28] and QuantumATK[29] software packages. In all the calculations performed with the QuantumATK code, all atoms were represented by a double-ζ-polarized (DZP) basis set, along with PseudoDojo norm-conserving pseudopotentials.[30] We have utilized the Perdew–Burke–Ernzerhof (PBE)[31] exchange-correlation (XC) functional, widely used in the determination of the transport properties of spin-crossover complexes in molecular junctions,[22, 23, 32] and the rPBE[33] functional, which has been shown to provide more accurate values for the gap between the HS-LS states in iron(II) spin-crossover complexes than other GGA functionals as the PBE.[34] The mesh cut-off energy was set to 210 Rydberg for both the real and reciprocal space grids in all calculations, with a self-consistency tolerance for the convergence of the Hamiltonian and density matrices of 1.0×10^{-4} eV.

In both the WFT and DFT calculations using the ORCA software package, all atoms were represented with a def2-TZVP[35] basis set, with the exception of the Fe ion, where a larger def2-QZVPP basis set was employed. The WFT calculations were carried out through the complete active space self-consistent field (CASSCF) methodology.[36] To consider the effects of the dynamic correlation, we employed the N-Electron Valence State Perturbation Theory (NEVPT2)[37] in its partially contracted formulation,[38] (FIC-NEVPT2 option in ORCA code). The converged CASSCF wavefunction was utilized as the reference, and the D3tpre and D4tpre parameters were set strictly to 0. For all calculations, the resolution of the identity (RI)[39] and the zeroth-order regular approximation (ZORA)[40] were adopted to increase the efficiency of the calculations and treat relativistic effects, respectively. The active space utilized in the CASSCF/NEVPT2 calculations consists of 10 electrons in 12 orbitals corresponding to six electrons occupying the five 3d-type orbitals centred on the Fe ion with their corresponding five "double-shell orbitals," and four electrons in two σ-type orbitals localized between the Fe centre and the six coordinating nitrogen atoms (Figures S2.1 and S2.2). This CAS (10,12) is commonly employed in CASSCF/PT2 studies on Fe(II) SCO complexes.[41-44]

Transport properties of the complexes and ligands

The transport properties of the complexes, as well as all geometry optimizations involved in the construction of the junctions, were obtained using the QuantumATK software package. These calculations

were performed employing the PBE-XC functional, and the same basis set and convergence parameters as in the single complex studies (see above) were used.

The molecular junctions (see Figure 2 for a representative example) were constructed starting with the full geometry relaxation of complexes 1 and 2, in both the HS and LS configurations, anchored to two Au(111) electrodes, by means of both terminal S groups bonded to two gold adatom in the hollow position of the surface. The unit cell was periodic in the three directions. It consisted of the complex between two 7x6 Au(111) slabs, three layers deep on one side and two layers deep on the other, thus keeping five Au layers (approximately 14 Å) between the periodic repetitions of the complex in the transport direction and a distance of about 11 Å in transverse ones. During all geometry optimizations, the unit cell size was allowed to relax in the transport direction and kept fixed in transverse ones. Finally, for the calculations of the transport properties, both Au(111) surfaces were reduced to slabs of 5x4 atoms, adding the corresponding vacuum space in the transverse directions to preserve a distance greater than 10 Å between the periodic images. The spin-resolved transport properties were computed using the combination of the DFT with the Keldysh nonequilibrium Green's function (NEGF) formalism, known as the DFT-NEGF methodology.[45-47]

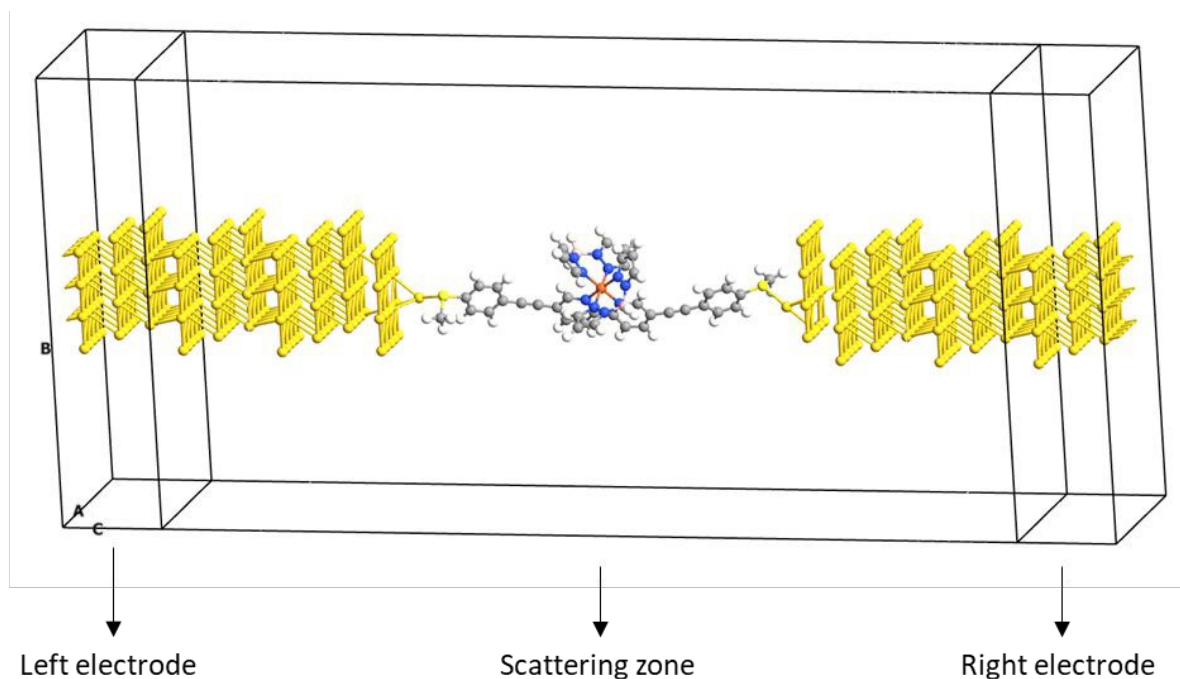Left electrode   Scattering zone   Right electrode

Figure 2. Scheme of the molecular junction architecture employed to study the spin-resolved transport properties of complex 1.

Under a finite bias voltage V_b, the spin-resolved current through the junction is given by the Landauer-Büttiker formula:[48]

$$I_\sigma(V_b) = \frac{e}{h}\int_{\mu_L}^{\mu_R} dE\; T_\sigma(E,V_b)[f_L(E,\mu_L) - f_R(E,\mu_R)]$$

where $\sigma = \alpha, \beta$ is the spin index, and $f_{L/R}$ and $\mu_{L/R}$ are the Fermi distribution function and chemical potential, respectively, of the left (L) or right (R) electrode. The spin-resolved transmission coefficient is defined by:

$$T_\sigma(E,V_b) = Tr[\Gamma_L G^r \Gamma_R G^a]$$

where G^r and G^a are the retarded and advanced Green´s functions, and $\Gamma_{L/R}$ is the self-energy matrices, which describe the coupling between the electrodes and the central scattering region.

The spin filtering efficiency at a given bias voltage is defined as:[49,50]

$$SFE(V) = \frac{|I_\alpha(V_B) - I_\beta(V_B)|}{I_\alpha(V_B) + I_\beta(V_B)},$$

and at zero bias:

$$SFE(V=0) = \frac{|T_\alpha(V=0) - T_\beta(V=0)|}{T_\alpha(V=0) + T_\beta(V=0)},$$

where $I_\alpha(I_\beta)$ and $T_\alpha(T_\beta)$ stands for the spin up (down) current and spin up (down) transmission, respectively, at zero bias.

Results and Discussion

Syntheses and characterization of the ligands and complexes

Ligands L1 and L2 were synthesized from the corresponding diethynyl-2,2'-bipyridine precursors, as depicted in schemes S1.1 and S1.2. Treatment of L1 with the charge-neutral iron(II) precursor complex, [Fe(H$_2$Bpz$_2$)$_2$(MeOH)$_2$],[51] yielded complex 1 as a greenish-yellow precipitate in a moderate yield. On the other hand, our attempts to obtain complex 2 in its pure form by treating L2 with the iron(II) precursor complex was not successful. To circumvent the issue, we propose the following. It has been reported in the literature that chemistry can be performed at the single molecular level, especially in molecular

junction forming experiments.[52,53, 54] Based on such reports, we propose direct trapping of complex 2 in between electrodes by treating a solution containing it above an electrode in a mechanically controllable break junction (MCBJ) and inducing contact formation by breaking the electrode. However, such experiment at the single-molecule level still needs to be performed; therefore, our suggestion is speculative in nature. Note, the complex formation reaction upon treatment of charge neutral iron(II) complex precursor—[Fe(H$_2$Bpz$_2$)$_2$]—and ligand L2 involves a colour change of the reaction mixture from pale yellow to green, and one can safely assume the expected complex formation by monitoring the colour change. Moreover, DFT-based thermochemistry calculations performed on complex 2 (Section S1.2 of the supporting information), shows that the compound is thermodynamically stable, supporting the hypothesis presented above. For more details on the preparation and characterization of L1, L2, and complex 1 and attempted preparation of complex 2, see supporting information (sections S1.1 and S1.2).

Spin-state switching characteristic of complex 1 in the bulk state

Complex 1 showed gradual and incomplete spin-state switching characteristics in the bulk powder state (Figure 3). At 300 K, a χT value of 3.05 cm^3 mol^{-1} K was observed indicating the HS state of the complex. Upon cooling at a scan rate of 3 K/min (cycle 1), the complex remained in the HS state until about 225 K. Afterwards, a gradual HS-to-LS switching started and proceeded until 60 K. Subsequently, a plateau-like region extending down to 30 K (χT = 1.92 cm^3 mol^{-1} K) was observed indicating the stabilization of a mixed phase with 2:1 HS/LS ratio. Cooling below 25 K resulted in a sudden decrease of the χT value to 1.2 cm^3 mol^{-1} K, attributed to the depopulation of the exited zero-field split levels of the HS term. In the heating branch, the χT versus T plot retraced the cooling branch until 64 K. After that a small lag in the LS-to-HS switching was observed in a narrow temperature range resulting in the formation of a small hysteresis loop (ΔT$_{1/2}$ = about 6 K). After crossing the hysteretic region, the switching profile retraced the heating branch. The observed lag in the LS-to-HS switching in the heating branch could have arisen due to the kinetic trapping of the LS complexes in the mixed phase. To check for the role of scan rate on the spin-state switching process, a second cycle was performed at a scan rate of 1 K/min. The switching proceeded exactly the same manner as observed for the 3 K/min scan rate, indicating the scan rate independent nature of the spin-state switching process until 1 K/min. The scan rate-dependent studies also confirm the reproducibility of the switching process.

On a comparative scale, stark differences in the spin-state switching characteristic of complex 1 and the parent [Fe(H$_2$Bpz$_2$)$_2$(2,2′-bipyridine)] complex (complex 3) have been observed. Complex 3 undergoes nearly complete spin-state switching with a T$_{1/2}$ = 160 K. On the contrary, complex 1 undergoes incomplete

spin-state switching with $T_{1/2}$ situated around 80 K, indicating the blocking of the SCO due to intermolecular interactions, as observed for [Fe(Me$_2$-H$_2$Bpz$_2$)$_2$(2,2′-bipyridine)] reported in the literature.[55]
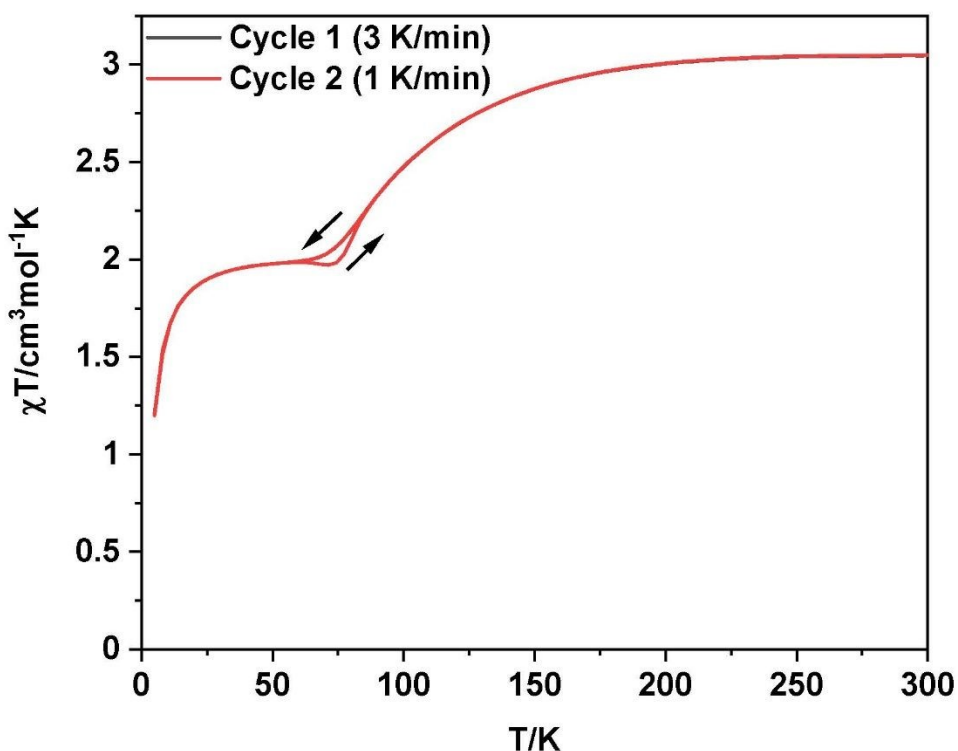

Figure 3. χT versus T plot of complex 1. Cycles 1 and 2 were performed at scan rates of 3 K/min and 1 K/min, respectively.

The preceding paragraph discusses the spin-state switching of complex 1 in the bulk state, which is governed by intermolecular interactions. On the other hand, intermolecular interactions no longer exist at the single-molecule level, and the switching between the spin-states is induced by a variety of mechanisms. Application of gate-voltage, electric field, and stretching of a molecule are all used to effect spin-state switching at the single-molecule level. It is worth noticing that despite complex 1 shows incomplete spin-state switching in the bulk state, a complete switching can still be induced by applying a suitable external stimulus at the single-molecule level, as rationalized below.

In general, SCO is considered as a bulk phenomenon dealing with cooperative intermolecular interactions. Such dependence of SCO on intermolecular interactions results in a myriad of factors controlling the nature of the spin-state switching. Therefore, the SCO phenomenon is mostly studied in the bulk state

and, to an extent, in the thin-film state. On the other hand, the well-studied prototypical [Fe(2,2`-bipyridine)$_3$]$^{2+}$ and its derivatives are known to undergo photo-induced LS-to-HS switching in solution at the single-molecule level via an intersystem crossing mechanism,[56,57,58] which is unusually fast for an optical process involving spin-multiplicity change.[59]

Apart from the photo-induced SCO discussed above, spin-state switching is also induced at the single-molecule level in molecular junctions by applying mechanisms such as stretching and electric field.[60,2] Examples include reports by Mayor and co-workers.[16,61] Ideally speaking, the complexes studied by Mayor and co-workers are not SCO active in the bulk state. Nevertheless, spin-state switching is still induced at the single-molecule level by applying mechanical and electric field stimuli. Based on the above arguments, we come to the following conclusion. Though complex 1 undergoes partial spin-state switching in the bulk state, such switching is not a bottleneck progressing towards the single-molecule switching realm, where operational principles are different compared to the bulk. As demonstrated below, spin-state switching of complex 1 can be induced at the single-molecule level by subjecting it to an electric field stimulus.

Electronic and magnetic properties of the complexes

Employing the geometry adopted by complex 1 and 2 in the molecular junction architectures for each spin state (see computational details section), we determined the energy difference between the HS (S=2) and LS (S=0) configurations of the isolated compounds ($\Delta E = E_{HS}-E_{LS}$), by performing DFT and WFT calculations. In addition, we have also calculated the HS-LS energy gap in the [Fe(H$_2$Bpz$_2$)$_2$(bipy)] reference complex 3, whose transition temperature (T$_{1/2}$ = 160 K), enthalpy (ΔH = 13.4 kJ mol^{-1}), and entropy (ΔS = 83.9 J mol^{-1} K^{-1}) variations upon SCO have been experimentally determined.[17] It is important to note that the geometry used for complex 3 in our calculations is the same one adopted by complex 1 in the junction after removing the anchoring and bridging groups. No further structure optimization has been performed, as this could affect the HS-LS energy difference when compared to the available experimental data for complex 3 in the bulk. The complete description of the details and results (XC functionals and software dependencies) of the studies can be found in section S2.2 of the supporting information.

For the three systems, all the calculations predict that the LS state is more stable than the HS state (Table S2). WFT calculations yield markedly reduced ΔE values compared to the DFT values. This fact is in line with previous computational studies dealing with SCO complexes,[34, 62, 63] where a significant overestimation of the calculated ΔE values is reported when DFT-based methods are employed, relative to the available experimental transition enthalpy values.

The CASSCF/NEVPT2 calculations estimate HS-LS gaps (ΔE) of 13.2, 7.1, and 11.3 kJ/mol for complexes 1, 2, and 3, respectively, in reasonable agreement with the transition enthalpy reported for iron(II) SCO complexes.[64]

Electric-field-induced spin-state switching of the complexes

Temperature-induced spin-state switching of iron(II) complexes in the bulk-state is a well-known phenomenon, and such switching can be induced easily either by heating or cooling the sample. On the other hand, triggering the spin-state switching at the single-molecule level, for example, by using stimulus such as electric-field or stretching, require cutting edge experimental techniques. Nevertheless, studies at the single-molecule level have been carried out to elucidate the utility of the SCO complexes as molecular spintronics components.[23,65,16] Considering the fact that one of the goals of this study is to elucidate how spin-state variation affects charge and spin transport characteristics in single-molecule junctions of 1 and 2, it is imperative to elucidate that the spin-state switching can be induced at the single-molecule level, before proceeding to transport calculations. To do so, we have computationally studied the effect of the electric field, produced by the voltage applied to the electrodes, on the HS-LS barrier of the isolated complexes. To this end, we have computed the energy of the HS and LS configurations by applying an electric field parallel to the transport direction in the junction (along the x axis). The electric field dependence of the HS-LS gaps for the complexes is shown in Figure 4a. For complex 1, the main component of the dipole moment in both spin states lies along the y axis, with a small component on the transport direction (x axis), with a different sign for the LS (positive) and HS (negative) states (Table S3). A positive electric field on the x axis favours the LS state and destabilizes the HS one, increasing the HS-LS separation. A negative electric field has the opposite effect; that is, the HS state is favoured. For a certain strength, the LS and HS states are degenerate, and the spin-state switching can be induced by the external electric field. In the case of complexes 2 and 3, the component of the dipole moment along the x axis has the same sign and very similar magnitude for both states. Consequently, application of electric field along the x axis does not modify the HS-LS separation for the particular orientation considered in our calculations. However, if complex 2 is oriented differently, for instance, slightly rotated due to non-symmetric contacts with the electrodes, both the x and y components of the dipole moment can interact with the external field, and favour the LS-HS switching. Experimental results support the viability of this electric field-assisted switching of iron(II) SCO complexes.[66-69] In addition, a recent theoretical study confirms the strong dependence of the electric field orientation with respect to the molecular dipole moment, in the voltage-induced HS-LS gap tuning.[70]
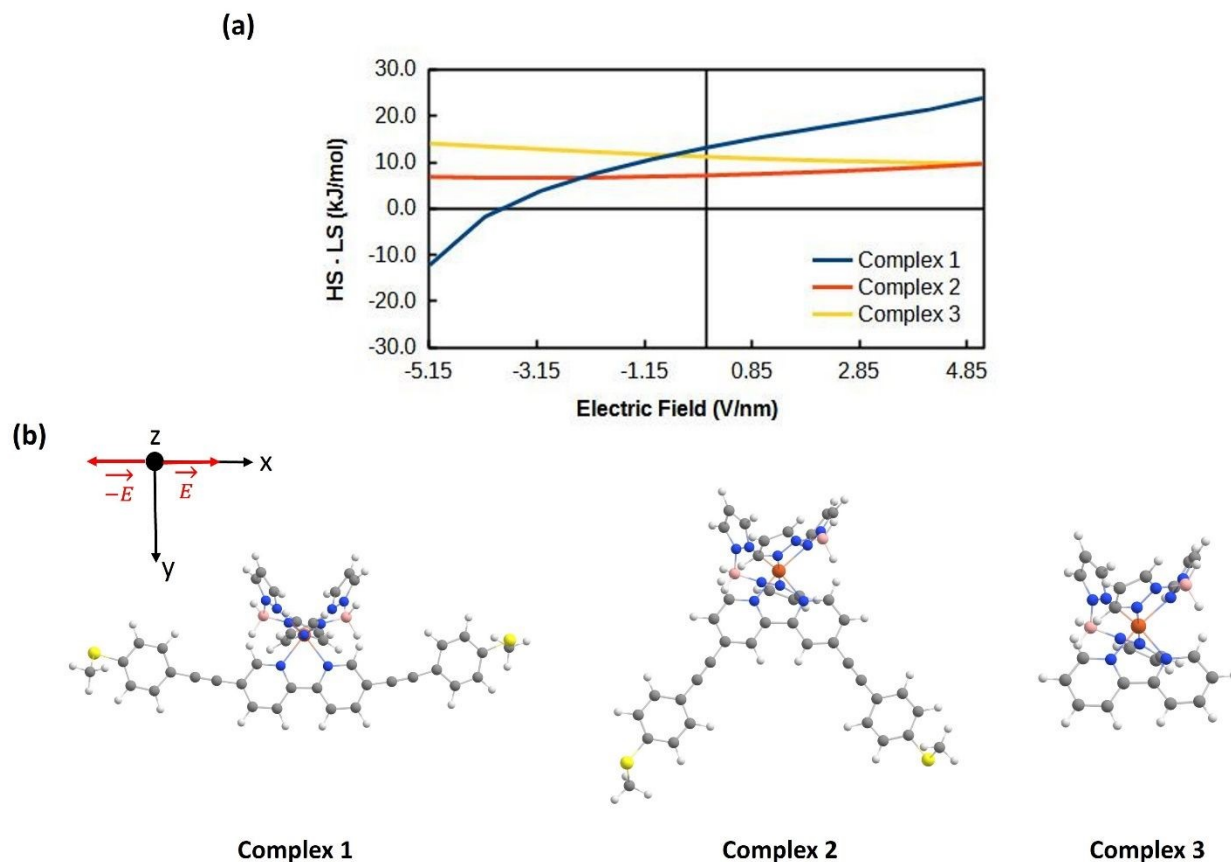
(a)

(b)

Figure 4. **(a)** Electric-field-dependent HS-LS energy gap on the three studied complexes evaluated through the CASSCF/NEVPT2 methodology. (b) Orientation of the applied electric field with respect to the molecular frame.

Transport properties of the complexes and ligands

Employing the fully optimized molecular junctions featuring complex 1 and 2 in HS and LS configurations (See computational details section), we probed the spin-resolved transport properties of the two compounds through the DFT-NEGF methodology. Also, we evaluated the transport properties of ligands L1 and L2 to establish the role that these moieties and the position of the anchoring moieties in the bipyridine skeleton play in the electronic transport. To this end, we built our computational models from the optimized geometry of complexes 1 and 2 in the LS state, removing the $[Fe(H_2Bpz_2)_2]$ fragment. In this way the resulting junction has exactly the same orientation and contacts with the electrodes as in the junctions containing the iron(II) complexes. This allows us to rationalize the dependence of the transport

properties on the position of the anchoring ligand without introducing any additional distortions of the molecular junction geometry.

Finally, to obtain more insights into the transport mechanisms, we performed an orbital-based analysis of the transport in the junctions, computing the transmission eigenfunctions at the resonance energies in the transmission spectrum, as well as the bridging molecule frontier orbitals under the influence of the electrodes, through the molecular projected self-consistent Hamiltonian (MPSH) states. These states are obtained by diagonalizing the molecular part of the full self-consistent Hamiltonian of the molecular junction device.

We start by discussing the results obtained for the junctions composed of complexes 1 and 2 in the HS configuration. The spin-resolved transmission spectra, projected density of states (PDOS) on the bridging complexes, and the transmission eigenfunctions computed at relevant energy points are depicted in Figure 5. Detailed figures of the transmission functions with the corresponding resonant molecular orbitals can be found in section S3 of the SI. Comparing the transmission eigenfunctions with the corresponding molecular frontier orbitals of complex 1 (Figure 5 insets, and Section S3 of the SI), we can establish that for the spin-up channel, the strongest signal (0.232 eV) is the product of the resonance with the spin-up lowest unoccupied molecular orbital (LUMO). In the spin-down case, the two prominent peaks stem from the resonances with the spin-down highest occupied molecular orbital (HOMO) (-0.096 eV) and the LUMO +1 (0.352 eV). It can be observed that the three molecular orbitals mentioned above have major contributions from the bipyridine moiety; the two spin-down ones also have contributions from one of the Fe 3d t_{2g}-like orbitals. In contrast, the spin-down LUMO (Figure S3.1) is totally localized in the Fe ion, not allowing a suitable coupling to the electrodes and thus not producing any transmission signal. Concerning the transport properties of complex 2, it can be seen that the peaks are much weaker than for complex 1. As in complex 1, the two closest signals to the Fermi level result from the resonance with spin-down HOMO and the spin-up LUMO (Figures S3.2 and S3.3). This decrease in the transmission signals is reflected on the zero-bias conductance values of both systems— junction featuring complex 1 exhibits spin-up and spin-down conductance values of $4.3 \times 10^{-3} G_0$ and $7.0 \times 10^{-3} G_0$, respectively. Whereas, spin-up and spin-down conductance values of $3.0 \times 10^{-6} G_0$ and $3.1 \times 10^{-4} G_0$, respectively, are computed for complex 2-based junction. Furthermore, the nature of the transmission eigenfunctions is essentially the same in both complexes; that is, they are mainly localized in the bipyridine moiety. A non-negligible contribution of the Fe d-type orbitals in the spin-down case was observed (see section S3 of the SI). It should be noticed that the distance between the electrodes is significantly shorter for the junction

with complex 2 (20.3 Å between the Au adatoms) than for the junction with complex 1 (27.3 Å). Therefore, the strong impact observed on the conductance is due to the position of the anchoring ligands, a fact that will be confirmed later while discussing the transport properties of the complexes in LS configuration and ligands L1 and L2.
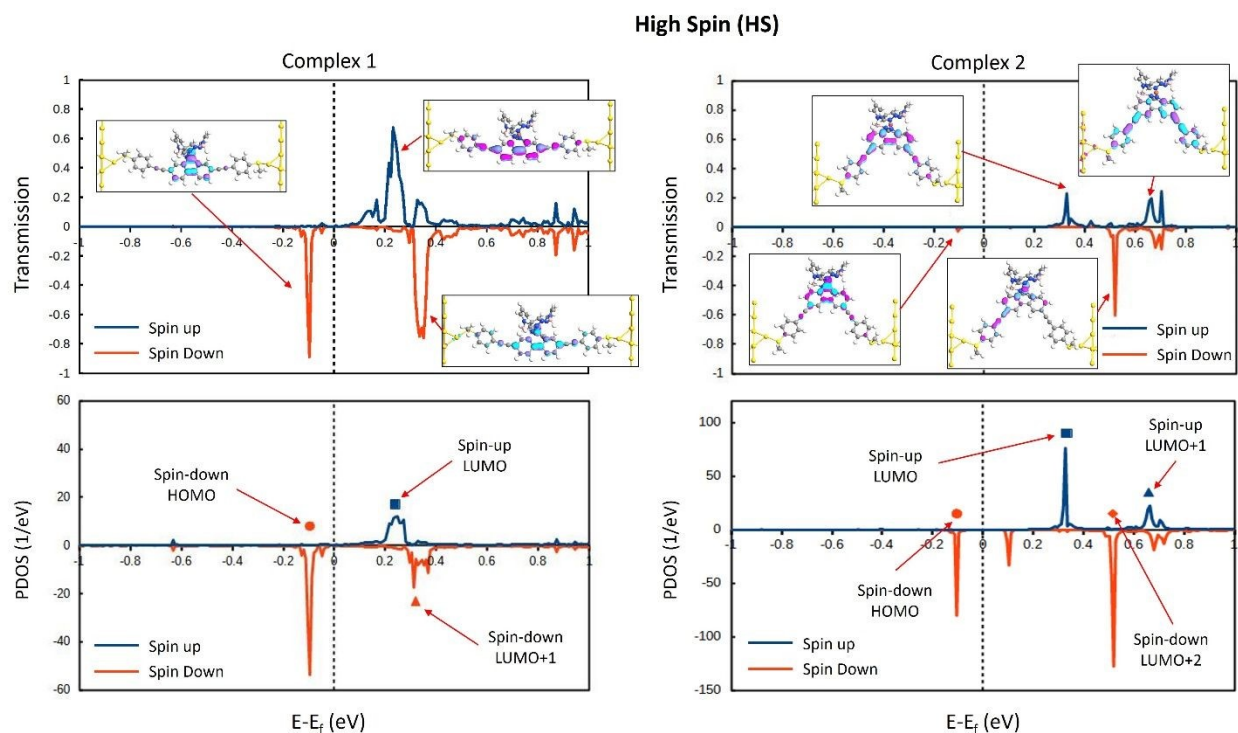

Figure 5. Spin resolved transmission spectra and PDOS on the molecular bridge utilizing complex 1 (Left) and complex 2 (Right) in the HS configuration as active elements. The insets in the transmission spectrum show the transmission eigenfunctions at the indicated peaks positions.

Next, we evaluate the transport properties of the HS junctions under an applied bias. Starting with the junction featuring complex 1, it can be observed that in a low bias voltage range (from 0 to 0.3 V), the spin-down current steeply increases while the spin-up one stays relatively constant, enhancing the SFE from 24% at 0 V to 80% at 0.3 V. This behaviour is attributed to the presence of the strong spin-down signal product of the resonance with the complex spin-down HOMO near the Fermi level, as mentioned above. Nevertheless, at an applied voltage of about 0.4 V, an abrupt drop in the spin-down current is observed. Subsequently, the current increased with increasing bias. To obtain more insight into this anomaly, we computed the transmission spectra and MPSH states in the junction at different applied bias voltages (Figure S4.1). It can be inferred from Figure S4.1 that the position of the spin-down HOMO is progressively displaced towards the junction Fermi level as the bias voltage increases. This displacement

heavily affects the transmission probability, as seen in the transmission spectra for the different voltage values. However, the form of this orbital and the corresponding transmission function produced by its resonance remain virtually unchanged (Figures S4.3 and S4.4).

The decrease in the magnitude of the transmission peaks and broadening observed for complex 2 is reflected in the I versus V profiles, where the spin-down current is about an order of magnitude smaller for complex 2, and nearly three orders of magnitude smaller for the spin-up case (Figure 6b). The dramatic decrease in the spin-up current yields an SFE of almost 100% over the entire voltage range studied. It is worth mentioning that the anomaly observed in the case of complex 1, where the spin-down current drastically drops above 0.3 V, is also present in the junction composed of complex 2 (from V > 0.4 V). However, in the case of complex 2, the current does not increase again, but it continues to drop until 0.6 V, exhibiting a negative differential resistance (NDR) effect. Moreover, a marked applied voltage-dependent displacement of the spin-down HOMO is also observed (Figure S4.2). Several of the features present in the I versus V profiles of the complexes—for example, the strong spin-down polarization of the current, highly bias-dependent transmission spectra, and NDR effects, have been reported in previous theoretical studies detailing the spin-polarized transport properties of iron(II) SCO complexes utilizing Au(111) nanowires as electrodes.[32, 71] Regarding the mechanisms underlying the NDR, a recent DFT-NEGF-based study suggests[72] that the local electronic structure of the electrodes could lead to the appearance of artificial NDR effects. Without discarding an artefact of the model itself, the observed NDR effect may be associated with a physical effect related to the displacement of molecular states close to the Fermi level under the effect of bias. This displacement could take the aforementioned molecular states into energy regions where the electrodes DOS drastically drops, decreasing the coupling with the electrodes and, thus, reducing the transmission. Also, both complexes exhibit a high SFE, in line with the values obtained for other iron(II)-based single-molecule junctions,[22, 23, 60, 73] in contrast to devices based on different transition metal—Co(II), Cr(II)— complexes that display much lower SFE values.[74, 75]
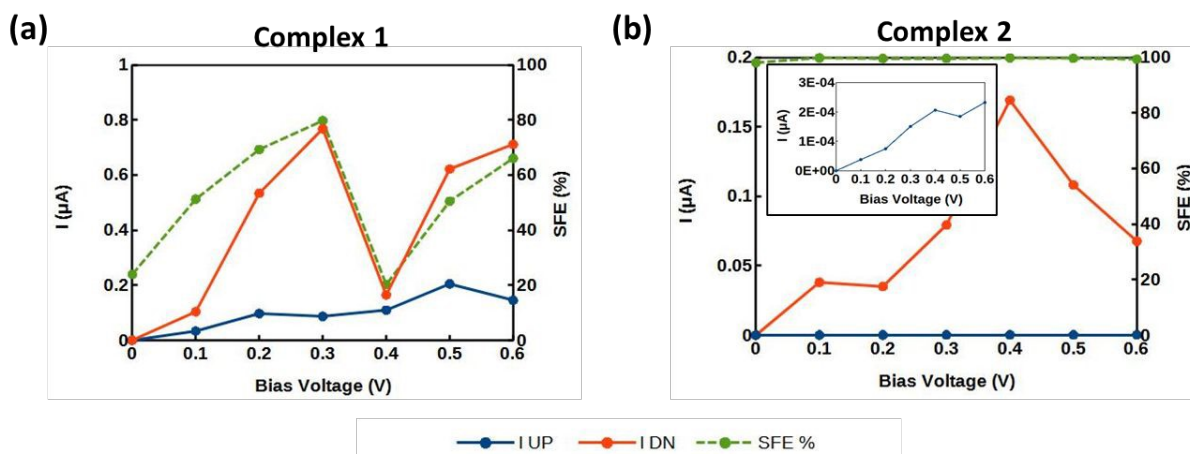
Figure 6. Spin-resolved current and SFE calculated in the junctions with (a) complex 1 and (b) 2 in HS configuration. The inset in (b) shows the detail of the spin-up current.

Finally, we report the results obtained for the ligands L1 and L2, and their respective complexes in the LS configuration. Their transmission spectra, PDOS plots, and relevant transmission functions are presented in Figure 7 and sections S5 and S6 of the SI. For both complexes and ligands, the strongest transmission signal arises from the resonance with the molecular bridge LUMO junctions. For complex 2 and ligand L2, an additional but weaker transmission peak is observed, product of the resonance with the molecule's LUMO+1 orbital. For the complexes, the transmission functions are mainly localized on the bipyridine and the anchoring ligands, exhibiting practically the same nature as those of the corresponding ligands. It is worth mentioning that the presence of the Fe(II) ion does not increase the intensity of the signals, but it displaces them by about 0.1 eV towards the Fermi level. The similarities between the transport properties of the ligands and their respective LS complexes are also reflected in their I-V profiles (Figure 8), and the computed zero-bias conductance values, $2.4 \times 10^{-6}\ G_0$ ($1.6 \times 10^{-6} G_0$) for complex 1 (L1), and $9.1 \times 10^{-7} G_0$ ($5.0 \times 10^{-7} G_0$) for complex 2 (L2). The calculated current values are very close for voltage values up to 0.5 V for L1 and complex 1 and 0.4 V for L2 and complex 2. The current in the junctions featuring the complexes drastically increases at higher voltages. Note that the zero-bias conductance for complex 1 and L1 is approximately 2 orders of magnitude higher than for complex 2 and L2, and the magnitude of the total current (spin-up + spin-down) is 3 orders of magnitude higher in all the studied voltage ranges (Figure 8), confirming that the position of the anchoring groups chiefly determines the conductance of the junction. It is also instructive to compare the conductance and total current in the junctions with the complexes in the HS configuration with the ones calculated for the ligands (Figure 8). For both ligands, iron(II) complexation significantly increases the total conductance/current, especially in the cases of

complex 2 and L2, where the conductance increases 3 orders of magnitude, and the total current from 2 to 3 orders of magnitude as the voltage is increased. This is in contrast to the behaviour observed for the complexes in the LS configuration, where the complexation of the ligands with the iron(II) containing fragment does not significantly increase the calculated conductance or total current. The higher conductance of the HS junctions has been reported in several experimental studies featuring iron(II) SCO complexes as molecular bridges.[16, 21, 76] To obtain more insight into the physical mechanism behind the drastic difference in the conductance of both complexes, we computed the pathway of the strongest peak in the transmission spectrum of the LS configuration, corresponding to the resonance with the LUMO of the complex (Figure S6.3). In this analysis, the transmission coefficient is projected into local bond contributions between pairs of atoms,[77] thus giving us an idea of how the carriers traverse the scattering zone. It can be observed that in complex 1 junction, a smooth path is stablished through the bipyridine ligand, in contrast to complex 2, where a high level of reflection is observed at the plane between both pyridine moieties. Note the anticlockwise circulation at the pyridine fragments of complex 2, in contrast to the straight path followed by the carries in complex 1. As some authors have pointed out, the origin of this phenomenon could be attributed to the antiresonance produced by destructive quantum interference effects (QI).[78-80]
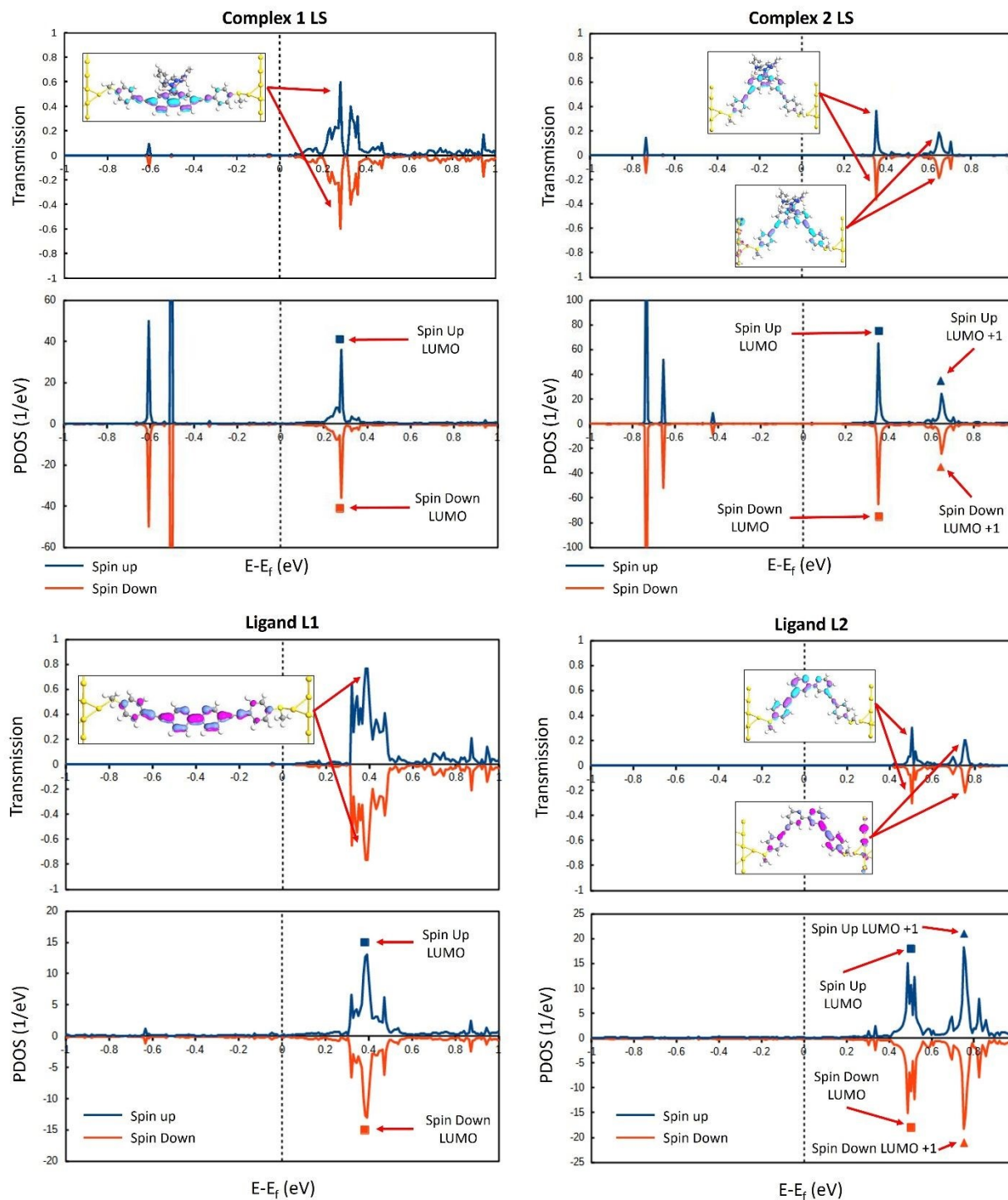
Figure 7. Spin-resolved transmission spectrum and PDOS on the molecular bridge utilizing ligands 1 and 2 as the junction active elements.
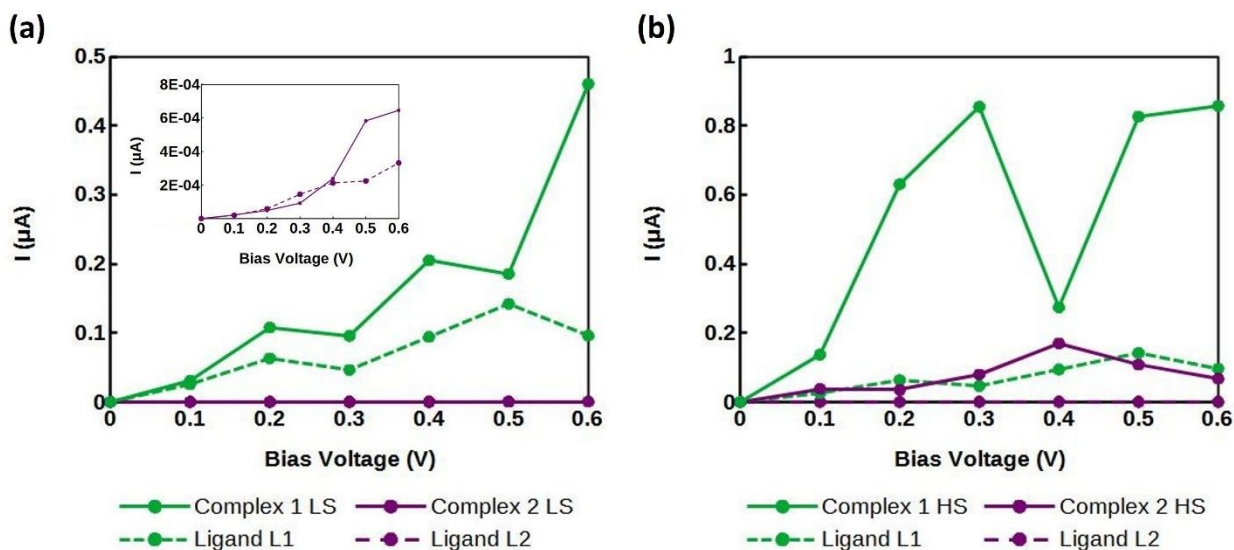
Figure 8. Comparison of the total current (spin-up + spin-down) versus bias voltage for ligands L1, L2 and complexes 1 and 2, in (a) LS and (b) HS configurations.

We would like to remark that the transport characteristics reported for complexes 1 and 2 in this study may not reflect the scenario in a realistic metal-molecule junction, where a myriad of metal-molecule bonding configurations are possible. On a comparative scale, the current values in the µA range calculated for the single-molecule junctions of complexes 1 and 2 (Figure 8) are much greater than current values in the nA [2, 21, 61, 81] or pA[82] range, typically measured in the single-molecule junctions of molecules undergoing spin-state switching. We attribute such high values of predicted current to the approximations associated with the computational methods applied to model transport in the single-molecule junctions of complexes 1 and 2. Remarkably, the current values calculated for 1 and 2 are in quantitative agreement with the calculated values reported for related SCO complexes at the single-molecule level,[3, 23, 83, 84] emphasizing on the role of methodology used to calculate the transport characteristics in over estimating the current values. Single-molecule transport measurements of [Fe(II)(H$_2$Bpz$_2$)$_2$(L)]-based complexes in MCBJ junctions are necessary to get insights into the true conductance values of the complexes.

Conclusions

In this computational investigation, we have studied the spin-state dependence of the charge and spin transport characteristics of single-molecule junctions composed of isomeric charge-neutral complexes 1 and 2. The WFT calculations revealed that spin-state switching of 1 can be triggered upon application of external electric field. On the other hand, complex 2 showed a weak applied electric field-dependent HS-

LS energy variation. Remarkably, small perturbations in the electrode-molecule coupling in the single-molecule junctions featuring complex 2 are shown to be effective in inducing electric-field-induced spin-state switching, auguring well for the experimental investigations. From the transport front, the DFT-NEGF calculations revealed the crucial role of the position of anchoring ligands in 1 and 2 in determining the total current (spin up + spin down). Both the HS and LS junctions of complex 1 showed higher conductance than the junctions of 2, and the variation of conductance is remarkably higher in the LS junctions than in the HS junctions. The isomeric nature of the complexes, culminating as different molecular orientations in the electrode gap, is also reflected on the spin-filtering efficiencies of the HS-junctions. While complex 1 exhibited voltage-dependent variation of SFE, complex 2 performed, theoretically, as an ideal spin filter (SFE ≈ 100%) over the studied voltage range. Our unsuccessful attempts to obtain complex 2 in its pure form is a limitation of the study. However, such limitation can be overcome by designing a new set of [Fe(II)(H$_2$Bpz$_2$)$_2$(bipy)]-based complexes featuring anchoring groups for metallic electrodes. We believe that the predictions presented in this study could serve as a starting point to study [Fe(II)(H$_2$Bpz$_2$)$_2$(bipy)]-based isomeric complexes.

Acknowledgments

Conflicts of interest

There are no conflicts of interest to declare.

References

(1) Venkataraman, L.; Klare, J. E.; Nuckolls, C.; Hybertsen, M. S.; Steigerwald, M. L. *Nature* **2006**, *442* (7105), 904-907. DOI: 10.1038/nature05037.

(2) Meded, V.; Bagrets, A.; Fink, K.; Chandrasekar, R.; Ruben, M.; Evers, F.; Bernand-Mantel, A.; Seldenthuis, J. S.; Beukman, A.; van der Zant, H. S. J. *Physical Review B* **2011**, *83* (24), 245415. DOI: 10.1103/PhysRevB.83.245415.

(3) Zhao, W.; Zou, D.; Yang, C.-L.; Sun, Z. *Journal of Materials Chemistry C* **2017**, *5* (34), 8862-8868, 10.1039/C7TC02312J. DOI: 10.1039/C7TC02312J.

(4) Liu, B.; Fu, H.; Guan, J.; Shao, B.; Meng, S.; Guo, J.; Wang, W. *ACS Nano* **2017**, *11* (11), 11402-11408. DOI: 10.1021/acsnano.7b06029.

(5) Godfrin, C.; Thiele, S.; Ferhat, A.; Klyatskaya, S.; Ruben, M.; Wernsdorfer, W.; Balestro, F. *ACS Nano* **2017**, *11* (4), 3984-3989. DOI: 10.1021/acsnano.7b00451.

(6) Halepoto, D. M.; Holt, D. G. L.; Larkworthy, L. F.; Leigh, G. J.; Povey, D. C.; Smith, G. W. *Journal of the Chemical Society, Chemical Communications* **1989**, (18), 1322-1323, 10.1039/C39890001322. DOI: 10.1039/C39890001322.

(7) Pandurangan, K.; Gildea, B.; Murray, C.; Harding, C. J.; Müller-Bunz, H.; Morgan, G. G. *Chemistry – A European Journal* **2012**, *18* (7), 2021-2029. DOI: https://doi.org/10.1002/chem.201102820.

(8) Gaspar, A. B.; Muñoz, M. C.; Niel, V.; Real, J. A. *Inorganic Chemistry* **2001**, *40* (1), 9-10. DOI: 10.1021/ic000788m.

(9) Naggert, H.; Rudnik, J.; Kipgen, L.; Bernien, M.; Nickel, F.; Arruda, L. M.; Kuch, W.; Näther, C.; Tuczek, F. *Journal of Materials Chemistry C* **2015**, *3* (30), 7870-7877, 10.1039/C5TC00930H. DOI: 10.1039/C5TC00930H.

(10) Gruber, M.; Miyamachi, T.; Davesne, V.; Bowen, M.; Boukari, S.; Wulfhekel, W.; Alouani, M.; Beaurepaire, E. *The Journal of Chemical Physics* **2017**, *146* (9), 092312. DOI: 10.1063/1.4973511 (acccessed 2022/04/05).

(11) Atzori, M.; Poggini, L.; Squillantini, L.; Cortigiani, B.; Gonidec, M.; Bencok, P.; Sessoli, R.; Mannini, M. *Journal of Materials Chemistry C* **2018**, *6* (33), 8885-8889, 10.1039/C8TC02685H. DOI: 10.1039/C8TC02685H.

(12) Miyamachi, T.; Gruber, M.; Davesne, V.; Bowen, M.; Boukari, S.; Joly, L.; Scheurer, F.; Rogez, G.; Yamada, T. K.; Ohresser, P.; et al. *Nature Communications* **2012**, *3* (1), 938. DOI: 10.1038/ncomms1940.

(13) Jasper-Toennies, T.; Gruber, M.; Karan, S.; Jacob, H.; Tuczek, F.; Berndt, R. *Nano Letters* **2017**, *17* (11), 6613-6619. DOI: 10.1021/acs.nanolett.7b02481.

(14) Tong, Y.; Kelaï, M.; Bairagi, K.; Repain, V.; Lagoute, J.; Girard, Y.; Rousset, S.; Boillot, M.-L.; Mallah, T.; Enachescu, C.; et al. *The Journal of Physical Chemistry Letters* **2021**, *12* (45), 11029-11034. DOI: 10.1021/acs.jpclett.1c03271.

(15) Mahfoud, T.; Molnár, G.; Cobo, S.; Salmon, L.; Thibault, C.; Vieu, C.; Demont, P.; Bousseksou, A. *Applied Physics Letters* **2011**, *99* (5), 053307. DOI: 10.1063/1.3616147 (acccessed 2022/06/10).

(16) Frisenda, R.; Harzmann, G. D.; Celis Gil, J. A.; Thijssen, J. M.; Mayor, M.; van der Zant, H. S. J. *Nano Letters* **2016**, *16* (8), 4733-4737. DOI: 10.1021/acs.nanolett.5b04899.

(17) Real, J. A.; Muñoz, M. C.; Faus, J.; Solans, X. *Inorganic Chemistry* **1997**, *36* (14), 3008-3013. DOI: 10.1021/ic960965c.

(18) Kuppusamy, S. K.; Spieker, L.; Heinrich, B.; Salamon, S.; Gruber, M.; Wende, H.; Ruben, M. *ChemRxiv* **2022**, *This content is a preprint and has not been peer-reviewed.* DOI: 10.26434/chemrxiv-2022-9mtbs.

(19) Kaliginedi, V.; V. Rudnev, A.; Moreno-García, P.; Baghernejad, M.; Huang, C.; Hong, W.; Wandlowski, T. *Physical Chemistry Chemical Physics* **2014**, *16* (43), 23529-23539, 10.1039/C4CP03605K. DOI: 10.1039/C4CP03605K.

(20) Chen, F.; Li, X.; Hihath, J.; Huang, Z.; Tao, N. *Journal of the American Chemical Society* **2006**, *128* (49), 15874-15881. DOI: 10.1021/ja065864k.

(21) Burzuri, E.; Garcia-Fuente, A.; Garcia-Suarez, V.; Senthil Kumar, K.; Ruben, M.; Ferrer, J.; van der Zant, H. S. J. *Nanoscale* **2018**, *10* (17), 7905-7911. DOI: 10.1039/c8nr00261d.

(22) Gu, Y.; Hu, Y.; Huang, J.; Li, Q.; Yang, J. *The Journal of Physical Chemistry C* **2019**, *123* (26), 16366-16372. DOI: 10.1021/acs.jpcc.9b02856.

(23) Aravena, D.; Ruiz, E. *Journal of the American Chemical Society* **2012**, *134* (2), 777-779. DOI: 10.1021/ja2090096.

(24) Bairagi, K.; Iasco, O.; Bellec, A.; Kartsev, A.; Li, D.; Lagoute, J.; Chacon, C.; Girard, Y.; Rousset, S.; Miserque, F.; et al. *Nature Communications* **2016**, *7* (1), 12212. DOI: 10.1038/ncomms12212.

(25) Shi, S.; Schmerber, G.; Arabski, J.; Beaufrand, J. B.; Kim, D. J.; Boukari, S.; Bowen, M.; Kemp, N. T.; Viart, N.; Rogez, G.; et al. *Applied Physics Letters* **2009**, *95* (4), 043303. DOI: 10.1063/1.3192355 (acccessed 2022/05/23).

(26) Warner, B.; Oberg, J. C.; Gill, T. G.; El Hallak, F.; Hirjibehedin, C. F.; Serri, M.; Heutz, S.; Arrio, M.-A.; Sainctavit, P.; Mannini, M.; et al. *The Journal of Physical Chemistry Letters* **2013**, *4* (9), 1546-1552. DOI: 10.1021/jz4005619.

(27) Gopakumar, T. G.; Matino, F.; Naggert, H.; Bannwarth, A.; Tuczek, F.; Berndt, R. *Angewandte Chemie International Edition* **2012**, *51* (25), 6262-6266. DOI: https://doi.org/10.1002/anie.201201203.

(28) Neese, F. *Wiley Interdisciplinary Reviews: Computational Molecular Science* **2012**, *2* (1), 73-78. DOI: 10.1002/wcms.81 (acccessed 2018/12/17).

(29) Smidstrup, S.; Markussen, T.; Vancraeyveld, P.; Wellendorff, J.; Schneider, J.; Gunst, T.; Verstichel, B.; Stradi, D.; Khomyakov, P. A.; Vej-Hansen, U. G.; et al. *Journal of Physics: Condensed Matter* **2019**, *32* (1), 015901. DOI: 10.1088/1361-648x/ab4007.

(30) van Setten, M. J.; Giantomassi, M.; Bousquet, E.; Verstraete, M. J.; Hamann, D. R.; Gonze, X.; Rignanese, G. M. *Computer Physics Communications* **2018**, *226*, 39-54. DOI: https://doi.org/10.1016/j.cpc.2018.01.012.

(31) Perdew, J. P.; Burke, K.; Ernzerhof, M. *Physical Review Letters* **1997**, *78* (7), 1396-1396. DOI: 10.1103/PhysRevLett.78.1396.

(32) Huang, J.; Xie, R.; Wang, W.; Li, Q.; Yang, J. *Nanoscale* **2016**, *8* (1), 609-616, 10.1039/C5NR05601B. DOI: 10.1039/C5NR05601B.

(33) Hammer, B.; Hansen, L. B.; Nørskov, J. K. *Physical Review B* **1999**, *59* (11), 7413-7421. DOI: 10.1103/PhysRevB.59.7413.

(34) Siig, O. S.; Kepp, K. P. *The Journal of Physical Chemistry A* **2018**, *122* (16), 4208-4217. DOI: 10.1021/acs.jpca.8b02027.

(35) Weigend, F. *Physical Chemistry Chemical Physics* **2006**, *8* (9), 1057-1065, 10.1039/B515623H. DOI: 10.1039/B515623H.

(36) Roos, B. O.; Taylor, P. R.; Si≐gbahn, P. E. M. *Chemical Physics* **1980**, *48* (2), 157-173. DOI: https://doi.org/10.1016/0301-0104(80)80045-0.

(37) Angeli, C.; Cimiraglia, R.; Evangelisti, S.; Leininger, T.; Malrieu, J. P. *The Journal of Chemical Physics* **2001**, *114* (23), 10252-10264. DOI: 10.1063/1.1361246 (acccessed 2022/06/06).

(38) Angeli, C.; Cimiraglia, R.; Malrieu, J.-P. *The Journal of Chemical Physics* **2002**, *117* (20), 9138-9153. DOI: 10.1063/1.1515317 (acccessed 2022/06/06).

(39) Neese, F. *Journal of Computational Chemistry* **2003**, *24* (14), 1740-1747. DOI: https://doi.org/10.1002/jcc.10318.

(40) Lenthe, E. v.; Baerends, E. J.; Snijders, J. G. *The Journal of Chemical Physics* **1993**, *99* (6), 4597-4610. DOI: 10.1063/1.466059 (acccessed 2018/12/17).

(41) Vela, S.; Fumanal, M.; Ribas-Ariño, J.; Robert, V. *Journal of Computational Chemistry* **2016**, *37* (10), 947-953. DOI: https://doi.org/10.1002/jcc.24283.

(42) Sousa, C.; de Graaf, C.; Rudavskyi, A.; Broer, R. *The Journal of Physical Chemistry A* **2017**, *121* (51), 9720-9727. DOI: 10.1021/acs.jpca.7b10687.

(43) Finney, B. A.; Chowdhury, S. R.; Kirkvold, C.; Vlaisavljevich, B. *Physical Chemistry Chemical Physics* **2022**, *24* (3), 1390-1398, 10.1039/D1CP04885F. DOI: 10.1039/D1CP04885F.

(44) Rudavskyi, A.; Sousa, C.; de Graaf, C.; Havenith, R. W. A.; Broer, R. *The Journal of Chemical Physics* **2014**, *140* (18), 184318. DOI: 10.1063/1.4875695 (acccessed 2022/05/25).

(45) Taylor, J.; Guo, H.; Wang, J. *Physical Review B* **2001**, *63* (24), 245407. DOI: 10.1103/PhysRevB.63.245407.

(46) Taylor, J.; Guo, H.; Wang, J. *Physical Review B* **2001**, *63* (12), 121104. DOI: 10.1103/PhysRevB.63.121104.

(47) Brandbyge, M.; Mozos, J.-L.; Ordejón, P.; Taylor, J.; Stokbro, K. *Physical Review B* **2002**, *65* (16), 165401. DOI: 10.1103/PhysRevB.65.165401.

(48) Büttiker, M.; Imry, Y.; Landauer, R.; Pinhas, S. *Physical Review B* **1985**, *31* (10), 6207-6215. DOI: 10.1103/PhysRevB.31.6207.

(49) Tao, L. L.; Wang, J. *Nanoscale* **2017**, *9* (34), 12684-12689. DOI: 10.1039/c7nr03532b.

(50) Zhao, P.; Gao, X.-J.; Song, Y.; Li, X.-X.; Chen, G. *Organic Electronics* **2018**, *57*, 104-109. DOI: https://doi.org/10.1016/j.orgel.2018.03.007.

(51) Ossinger, S.; Nather, C.; Tuczek, F. *IUCrData* **2016**, *1* (8), x161252. DOI: doi:10.1107/S2414314616012529.

(52) Xie, X.; Li, P.; Xu, Y.; Zhou, L.; Yan, Y.; Xie, L.; Jia, C.; Guo, X. *ACS Nano* **2022**, *16* (3), 3476-3505. DOI: 10.1021/acsnano.1c11433.

(53) Li, X.; Hu, D.; Tan, Z.; Bai, J.; Xiao, Z.; Yang, Y.; Shi, J.; Hong, W. *Topics in Current Chemistry* **2017**, *375* (2), 42. DOI: 10.1007/s41061-017-0123-x.

(54) Cao, Y.; Dong, S.; Liu, S.; He, L.; Gan, L.; Yu, X.; Steigerwald, M. L.; Wu, X.; Liu, Z.; Guo, X. *Angewandte Chemie International Edition* **2012**, *51* (49), 12228-12232, https://doi.org/10.1002/anie.201205607. DOI: https://doi.org/10.1002/anie.201205607 (acccessed 2022/11/29).

(55) Ossinger, S.; Näther, C.; Tuczek, F. *Journal of Physics: Condensed Matter* **2019**, *32* (9), 094001. DOI: 10.1088/1361-648x/ab5776.

(56) Zhang, W.; Alonso-Mori, R.; Bergmann, U.; Bressler, C.; Chollet, M.; Galler, A.; Gawelda, W.; Hadt, R. G.; Hartsock, R. W.; Kroll, T.; et al. *Nature* **2014**, *509* (7500), 345-348. DOI: 10.1038/nature13252.

(57) Bressler, C.; Milne, C.; Pham, V. T.; ElNahhas, A.; van der Veen, R. M.; Gawelda, W.; Johnson, S.; Beaud, P.; Grolimund, D.; Kaiser, M.; et al. *Science* **2009**, *323* (5913), 489-492. DOI: 10.1126/science.1165733 (acccessed 2022/09/28).

(58) Cannizzo, A.; Milne, C. J.; Consani, C.; Gawelda, W.; Bressler, C.; van Mourik, F.; Chergui, M. *Coordination Chemistry Reviews* **2010**, *254* (21), 2677-2686. DOI: https://doi.org/10.1016/j.ccr.2009.12.007.

(59) Oppermann, M.; Zinna, F.; Lacour, J.; Chergui, M. *Nature Chemistry* **2022**, *14* (7), 739-745. DOI: 10.1038/s41557-022-00933-0.

(60) Kuppusamy, S. K.; Mizuno, A.; García-Fuente, A.; van der Poel, S.; Heinrich, B.; Ferrer, J.; van der Zant, H. S. J.; Ruben, M. *ACS Omega* **2022**, *7* (16), 13654-13666. DOI: 10.1021/acsomega.1c07217.

(61) Harzmann, G. D.; Frisenda, R.; van der Zant, H. S. J.; Mayor, M. *Angewandte Chemie International Edition* **2015**, *54* (45), 13425-13430. DOI: https://doi.org/10.1002/anie.201505447.

(62) Cirera, J.; Via-Nadal, M.; Ruiz, E. *Inorganic Chemistry* **2018**, *57* (22), 14097-14105. DOI: 10.1021/acs.inorgchem.8b01821.

(63) Reiher, M. *Inorganic Chemistry* **2002**, *41* (25), 6928-6935. DOI: 10.1021/ic025891l.

(64) Kepp, K. P. *Inorganic Chemistry* **2016**, *55* (6), 2717-2727. DOI: 10.1021/acs.inorgchem.5b02371.

(65) Karuppannan, S. K.; Martín-Rodríguez, A.; Ruiz, E.; Harding, P.; Harding, D. J.; Yu, X.; Tadich, A.; Cowie, B.; Qi, D.; Nijhuis, C. A. *Chemical Science* **2021**, *12* (7), 2381-2388, 10.1039/D0SC04555A. DOI: 10.1039/D0SC04555A.

(66) Zhang, X.; Palamarciuc, T.; Létard, J.-F.; Rosa, P.; Lozada, E. V.; Torres, F.; Rosa, L. G.; Doudin, B.; Dowben, P. A. *Chemical Communications* **2014**, *50* (18), 2255-2257, 10.1039/C3CC46892E. DOI: 10.1039/C3CC46892E.

(67) Lefter, C.; Tan, R.; Dugay, J.; Tricard, S.; Molnár, G.; Salmon, L.; Carrey, J.; Nicolazzi, W.; Rotaru, A.; Bousseksou, A. *Chemical Physics Letters* **2016**, *644*, 138-141. DOI: https://doi.org/10.1016/j.cplett.2015.11.036.

(68) Minakova, O. V.; Tumanov, S. V.; Fedin, M. V.; Veber, S. L. *Russian Journal of Coordination Chemistry* **2020**, *46* (5), 326-329. DOI: 10.1134/S1070328420040041.

(69) Hao, G.; Mosey, A.; Jiang, X.; Yost, A. J.; Sapkota, K. R.; Wang, G. T.; Zhang, X.; Zhang, J.; N'Diaye, A. T.; Cheng, R.; et al. *Applied Physics Letters* **2019**, *114* (3), 032901. DOI: 10.1063/1.5054909 (acccessed 2022/06/29).

(70) Sánchez-de-Armas, R.; Montenegro-Pohlhammer, N.; Develioglu, A.; Burzurí, E.; Calzado, C. J. *Nanoscale* **2021**, *13* (44), 18702-18713, 10.1039/D1NR04577F. DOI: 10.1039/D1NR04577F.

(71) Li, F.; Huang, J.; Hu, Y.; Li, Q. *RSC Advances* **2019**, *9* (22), 12339-12345, 10.1039/C9RA01420A. DOI: 10.1039/C9RA01420A.

(72) Li, D.; Tong, Y.; Bairagi, K.; Kelai, M.; Dappe, Y. J.; Lagoute, J.; Girard, Y.; Rousset, S.; Repain, V.; Barreteau, C.; et al. *The Journal of Physical Chemistry Letters* **2022**, *13* (32), 7514-7520. DOI: 10.1021/acs.jpclett.2c01934.

(73) Yan, Q.; Zhou, L.; Cheng, J.-F.; Wen, Z.; Han, Q.; Wang, X.-F. *The Journal of Chemical Physics* **2016**, *144* (15), 154304. DOI: 10.1063/1.4946803 (acccessed 2022/06/29).

(74) Niu, L.; Wang, H.; Bai, L.; Rong, X.; Liu, X.; Li, H.; Yin, H. *Frontiers of Physics* **2017**, *12* (4), 127207. DOI: 10.1007/s11467-017-0671-0.

(75) Hu, Y.; Li, X.; Li, Q.; Yang, J. *Angewandte Chemie International Edition* **2022**, *n/a* (n/a), e202205036, https://doi.org/10.1002/anie.202205036. (acccessed 2022/06/29).

(76) Aragonès, A. C.; Aravena, D.; Cerdá, J. I.; Acís-Castillo, Z.; Li, H.; Real, J. A.; Sanz, F.; Hihath, J.; Ruiz, E.; Díez-Pérez, I. *Nano Letters* **2016**, *16* (1), 218-226. DOI: 10.1021/acs.nanolett.5b03571.

(77) Solomon, G. C.; Herrmann, C.; Hansen, T.; Mujica, V.; Ratner, M. A. *Nature Chemistry* **2010**, *2* (3), 223-228. DOI: 10.1038/nchem.546.

(78) Liu, J.; Huang, X.; Wang, F.; Hong, W. *Accounts of Chemical Research* **2019**, *52* (1), 151-160. DOI: 10.1021/acs.accounts.8b00429.

(79) Huang, B.; Liu, X.; Yuan, Y.; Hong, Z.-W.; Zheng, J.-F.; Pei, L.-Q.; Shao, Y.; Li, J.-F.; Zhou, X.-S.; Chen, J.-Z.; et al. *Journal of the American Chemical Society* **2018**, *140* (50), 17685-17690. DOI: 10.1021/jacs.8b10450.

(80) Jiang, F.; Trupp, D. I.; Algethami, N.; Zheng, H.; He, W.; Alqorashi, A.; Zhu, C.; Tang, C.; Li, R.; Liu, J.; et al. *Angewandte Chemie International Edition* **2019**, *58* (52), 18987-18993, https://doi.org/10.1002/anie.201909461. (acccessed 2022/09/21).

(81) Wagner, S.; Kisslinger, F.; Ballmann, S.; Schramm, F.; Chandrasekar, R.; Bodenstein, T.; Fuhr, O.; Secker, D.; Fink, K.; Ruben, M.; et al. *Nature Nanotechnology* **2013**, *8* (8), 575-579. DOI: 10.1038/nnano.2013.133.

(82) Johannsen, S.; Ossinger, S.; Markussen, T.; Tuczek, F.; Gruber, M.; Berndt, R. *ACS Nano* **2021**, *15* (7), 11770-11778. DOI: 10.1021/acsnano.1c02698.

(83) Huang, J.; Xie, R.; Hu, Y.; Lei, S.; Li, Q. *Chemical Physics Letters* **2020**, *758*, 137925. DOI: https://doi.org/10.1016/j.cplett.2020.137925.

(84) Liu, M.; Han, X.; Huang, H.; Long, X.; Tan, B. *Chemical Physics Letters* **2022**, *801*, 139682. DOI: https://doi.org/10.1016/j.cplett.2022.139682.